ROLE OF LOCAL GEOMETRY IN THE SPIN AND ORBITAL STRUCTURE OF TRANSITION METAL COMPOUNDS

D. I. Khomskii [a*], **K. I. Kugel** [b], **A. O. Sboychakov** [b], **S. V. Streltsov** [c,d]

[a] *II. Physikalisches Institut, Universität zu Köln*
50937, Köln, Germany

[b] *Institute for Theoretical and Applied Electrodynamics, Russian Academy of Sciences*
125412, Moscow, Russia

[c] *Mikheev Institute for Metal Physics, Russian Academy of Sciences, Ural Branch*
620990, Ekaterinburg, Russia

[d] *Ural Federal University*
620002, Ekaterinburg, Russia

We analyze the role of local geometry in the spin and orbital interaction in transition metal compounds with orbital degeneracy. We stress that the tendency observed in the most studied case (transition metals in O_6 octahedra with one common oxygen — common corner of neighboring octahedra — and with $\sim 180°$ metal–oxygen–metal bonds), that ferro-orbital ordering renders antiferro-spin coupling and, *vice versa*, antiferro-orbitals give ferro-spin ordering, is not valid in the general case, in particular, for octahedra with a common edge and with $\sim 90°$ M–O–M bonds. Special attention is paid to the "third case", that of neighboring octahedra with a common face (three common oxygens), which has largely been disregarded until now, although there are many real systems with this geometry. Interestingly enough, the spin–orbital exchange in this case turns out to be simpler and more symmetric than in the first two cases. We also consider which form the effective exchange takes for different geometries in the case of strong spin–orbit coupling.

Contribution for the JETP special issue in honor of L. V. Keldysh's 85th birthday

1. INTRODUCTION

The study of correlated systems with orbital ordering is currently a very active field of research in solid state physics. Orbital ordering not only is accompanied (or caused) by structural transitions, but also largely determines magnetic properties of many materials, e.g., transition-metal oxides: according to the Goodenough–Kanamori–Anderson rules [1], the orbital occupation largely determines the magnitude and even the sign of exchange interaction. By modifying orbital occupation, one can control magnetic properties of a system [2]. Besides more traditional electron–lattice (Jahn–Teller) mechanism [3] of orbital ordering, a purely electronic (exchange) mechanism can also lead

to both orbital and magnetic ordering [4], which appear to be coupled.

The coupled spin and orbital ordering depends not only on the electronic structure of constituent ions but also on the local geometry of the system. The most often treated case is the system with a transition metal ion (M) surrounded by the ligand (e.g., oxygen, O) octahedra, with these neighboring MO_6 octahedra having one common oxygen (common corner) with the M–O–M angle of about 180° (it may also be smaller than 180°, but small deviations of this angle from 180° do not play an important role; see, e.g., [5]). This situation is met, for example, in such important systems as perovskites, e.g., CMR manganites $(LaSr)MnO_3$ or in high-T_c cuprates like $(LaSr)_2CuO_4$. Much is known in this case: what form takes the electron–lattice (Jahn–Teller) interaction that leads to orbital ordering and how the spin exchange looks. The general conclusion reached in the study of these systems is that ferro-

* E-mail: khomskii@ph2.uni-koeln.de

orbital ordering usually leads to the antiferromagnetic spin ordering and *vice versa*, antiferro-orbital ordering gives rise to the ferromagnetic spin exchange. This "rule" became a kind of "folklore" and is used by many theoreticians and experimentalists to explain or predict the type of coupled spin and orbital ordering in various systems with different crystal structures. However, we must realize that this "rule" was derived for this particular geometry, and it does not have to be fulfilled in other cases. For example, it is not the case for neighboring MO_6 octahedra having two common oxygens (common edge) with the M–O–M angle of about 90°. There are a number of interesting and important materials with this local geometry, including the "battery material" $LiCoO_2$, many frustrated systems, multiferroics, etc. (we note that the deviations from the "pure" 90° M–O–M angle may have more drastic consequences here). As we discuss below (see also [5, 6]), this general "rule" is strongly violated in this case.

There also exists a much less studied "third case" of neighbors with three common oxygens, the systems with MO_6 octahedra sharing a common face. Understanding the systematics of coupled spin and orbital ordering in these different cases is an interesting and practically important problem, which is discussed in this paper.

In addition to the local M–O geometry, which is crucial for the superexchange originating from the virtual hopping of d electrons via ligands, e. g., oxygens, in the second and the third cases (common edge and common face), in contrast to the simpler case of a common corner, electron hopping leading to superexchange can occur not only via ligands: there may also exist a significant direct overlap of certain d orbitals of neighboring transition metal ions. The resulting direct exchange should also be taken into account in certain cases; it can lead to very nontrivial effects [6].

One more factor, important especially for heavy ($4d$, $5d$) transition metals and attracting much attention nowadays, is the role of the relativistic spin–orbit coupling, which for these elements could be very significant and which could sometimes dominate the properties of corresponding systems. In this paper, we consider these effects for different geometries.

The plan of the paper is as follows. In Secs. 2 and 3, we briefly summarize the known properties of spin and orbital exchange for the geometries with a common corner (the M–O–M angle of about 180°) and common edge (90° M–O–M bonds). In particular, we want to stress several important features that distinguish these two cases. We also compare the situation in these two cases for systems with strong spin–orbit cou-

pling. Then, in Secs. 4 and 5, we discuss the much less studied case of systems with a common face of neighboring MO_6 octahedra, partly using the results of our recent paper [7] and generalizing those to the case a finite noncubic crystal field and also to that of significant spin–orbit coupling. The details of calculations are given in Appendix.

2. SYSTEMS WITH THE COMMON-CORNER GEOMETRY

The geometry of systems with MO_6 octahedra sharing a common corner is illustrated in Fig. 1a. Here, the transition metals are rather far away from each other, with ligand (oxygen) ions in between. In such a situation, all electron hoppings occur via oxygens. We also show in Fig. 1b what the crystal field splitting is in the case of ideal octahedra. For the tetragonal reference frame with axes directed from M to O ions, the e_g orbitals are $|x^2 - y^2\rangle$ and $|3z^2 - r^2\rangle$, while the t_{2g} orbitals are $|xy\rangle$, $|yz\rangle$, and $|zx\rangle$.

In the simple case of one electron or one hole in a doubly degenerate e_g orbital (Cu^{2+} or low-spin Ni^{3+}), we can describe the state of an ion by the spin $S = 1/2$ and by the orbital occupation, which can also be mapped into pseudospin-1/2 situation, with the pseudospin projection $\tau^z = 1/2$ corresponding to orbital 1, say $|x^2 - y^2\rangle$, and $\tau^z = -1/2$ to orbital 2, $|3z^2 - r^2\rangle$. We can also make arbitrary linear superpositions of these states, of the type

$$\alpha|3z^2 - r^2\rangle + \beta|x^2 - y^2\rangle, \quad |\alpha|^2 + |\beta|^2 = 1,$$

where coefficients α and β can in principle be complex [8]. For one electron per site and in the strongly interacting case (with the Hubbard on-site electron repulsion U much larger than the electron hopping integral t), the usual treatment in the perturbation theory in t/U leads to the following schematic form of the exchange Hamiltonian:

$$H = J_1 \sum_{\langle ij \rangle} \mathbf{S}_i \cdot \mathbf{S}_j + \sum_{\langle ij \rangle} J_{2,ij}^{\alpha\beta} \tau_i^\alpha \tau_j^\beta + \\ + \sum_{\langle ij \rangle} J_{3,ij}^{\alpha\beta} (\mathbf{S}_i \cdot \mathbf{S}_j)(\tau_i^\alpha \tau_j^\beta), \quad (1)$$

where the summation is taken over the nearest-neighbor sites, $\mathbf{S}_i$ is the spin of site i, and the pseudospin operators $\boldsymbol{\tau}_i$ describe the orbital state in the case of double orbital degeneracy (say, for e_g levels). The spin part of this exchange is of a Heisenberg type ($\mathbf{S}_i \cdot \mathbf{S}_j$), but the orbital part may be more complicated,
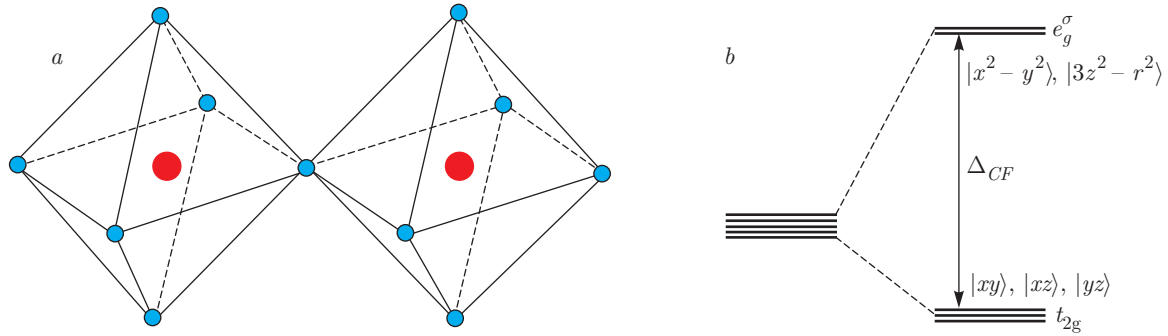
Fig. 1. (a) Corner-sharing octahedra: large and small circles respectively denote metal and ligand ions. (b) Crystal field (CF) splitting of d orbitals of the metal ion

containing anisotropic terms like $\tau_i^z \tau_j^z$, $\tau_i^x \tau_j^x$, $\tau_i^z \tau_j^x$, etc., which, in addition, depend on the relative orientation of sites i and j. Only in a more symmetric model (not actually realized for e_g states) with the effective d–d hopping such that $t_{11} = t_{22} = t$, $t_{12} = 0$ does the effective Hamiltonian take the simpler symmetric form [4]

$$H = J \sum_{\langle ij \rangle} \left(\frac{1}{2} + 2\mathbf{S}_i \cdot \mathbf{S}_j \right) \left(\frac{1}{2} + 2\boldsymbol{\tau}_i \cdot \boldsymbol{\tau}_j \right), \quad (2)$$

which has a rather high, not only $SU(2) \times SU(2)$, but even $SU(4)$ symmetry [9–11]. Similarly, one can obtain the effective spin–orbital model for triply degenerate t_{2g} electrons, which, instead of pseudospin-1/2 orbital operators $\boldsymbol{\tau}_i$, would contain effective orbital $l = 1$ operators, $\mathbf{l}_i$, describing three t_{2g} states [12]. In the general case, these operators enter not only as $\mathbf{l}_i\mathbf{l}_j$, but also with invariants of the type $l_i^z l_j^z - 2/3$ or $l_i^x l_j^y + l_i^y l_j^x$, etc.

As mentioned in the Introduction, in the doubly degenerate case for simple lattices such as that of perovskites AMO_3 with MO_6 octahedra having common corner (one common oxygen, with the M–O–M angle of $\approx 180°$, see Fig. 1a), the typical situation is that the ferro-orbital ordering gives rise to the antiferromagnetic spin exchange, whereas antiferro-orbital ordering is rather favorable for spin ferromagnetism. However, we must realize that this conclusion was reached in a particular case, for systems with particular geometry, with 180° M–O–M superexchange, and the situation is very different in other cases, as we demonstrate below.

We conclude this section by presenting the results for this geometry in the case of the strong spin–orbit coupling. The spin–orbit coupling is quenched for e_g electrons (see, e. g. [1, 5]), but the interesting and nontrivial results can occur for partially filled t_{2g} levels. However, just this is the typical situation for the 4d and 5d compounds for which spin–orbit coupling is strong: due to the large crystal field splitting $\Delta_{CF} = 10Dq$

and smaller Hund's energy (Hund's rule coupling J_H is 0.8–0.9 eV for 3d elements, 0.6–0.7 eV for 4d, and near 0.5 eV for 5d), these ions are usually in the low-spin state, i. e., their electrons first fill the t_{2g} levels, and only for $n_d > 6$ electrons start to occupy the e_g levels. In these cases, one can sometimes project electronic states to the ground-state multiplets calculated including spin–orbit coupling. Here, we have to discriminate between the cases with different electron occupation (a less-than-half-filled t_{2g} shell, $n_{t_{2g}} < 3$, and a more-than-half-filled shell, $n_{t_{2g}} > 3$). The second (or the third) Hund's rule for partially filled t_{2g} shells tells us that the ground state multiplet for $n_{t_{2g}} < 3$ corresponds to the maximum possible total momentum j, and for a more-than-half-filled t_{2g} shell, — to the minimum possible j. In effect, e. g., for dominating spin–orbit coupling, the ions with the d^5 configuration (Ir^{4+}, Os^{3+}) would have a Kramers doublet $j = 1/2$ as a ground state (for the t_{2g} triplet, $l_{eff} = 1$ and $S = 1/2$, which gives the $j = 1/2$ doublet as a ground state), which can be described by the effective spin $\sigma = 1/2$ (usual Pauli matrices) [5, 13]. The superexchange can then be projected onto this subspace and written through the pseudospin $j = 1/2$ operators. The form of this exchange for strongly localized electrons ($U > J_H \gg t$) has been obtained for perovskites with 180° exchange, e. g., Sr_2IrO_4, and for 90° exchange, e. g., for Na_2IrO_3, in Ref. [14]. The resulting exchange interaction in terms of $j = 1/2$ looks very different: it is predominantly Heisenberg-like for 180° bonds, but is strongly anisotropic (Ising-like) for each Ir–O–Ir pair in case of IrO_6 octahedra with common edge oxygens. Indeed, for corner-sharing octahedra, the dominant exchange has the simple Heisenberg form [14]

$$H = J \sum_{\langle ij \rangle} \boldsymbol{\sigma}_i \cdot \boldsymbol{\sigma}_j, \quad (3)$$

where $\boldsymbol{\sigma}$ are the Pauli matrices describing the effective spin $1/2$ for the $j = 1/2$ Kramers doublets. We see that the strong spin–orbit coupling can effectively remove orbital degeneracy, and instead of the complicated spin–orbital Hamiltonian of the type of Eqs. (1) or (2) (or an even more complicated form for the triple t_{2g} degeneracy; see above and Ref. [12]), we obtain the simple Heisenberg interaction (3). However, whether in real cases we indeed meet the situation in which the spin–orbit coupling dominates, is a special question, which should be addressed for each specific system.

3. SPIN-ORBITAL EXCHANGE FOR OCTAHEDRA WITH A COMMON EDGE

Another typical situation in transition-metal compounds is that with neighboring transition-metal ions having two common oxygens; for systems with MO_6 octahedra, this is the case of a common edge, with $\approx 90°$ M–O–M bonds, see Fig. 2 (instead of oxygens, there may be other ligands: halogens such as F, Cl, or S, Se, Te, etc.). This situation is typical, for example, for B sites of spinels, or in layered materials with CdI_2 or with delafossite structures, etc. In this case, the situation with spin–orbital exchange is quite different from that for octahedra with a common corner (see, e. g., [15] and the discussion below). For example, for e_g electrons, the exchange interaction is ferromagnetic for both ferro- and antiferro-orbital ordering. The effective superexchange interaction in the case of doubly degenerate e_g orbitals schematically has the form [15] (in the symmetric case)

$$H_{12} = -\tilde{J}\left(\frac{3}{4} + \mathbf{S}_1 \cdot \mathbf{S}_2\right)\left[\left(\frac{1}{2} + T_{x,1}^z\right)\left(\frac{1}{2} + T_{y,2}^z\right) + \left(\frac{1}{2} + T_{y,1}^z\right)\left(\frac{1}{2} + T_{x,2}^z\right)\right], \quad (4)$$
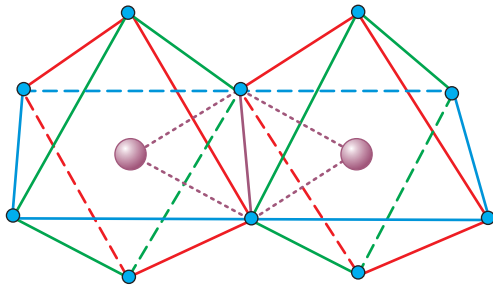
Fig. 2. Edge-sharing octahedra. Large and small circles respectively denote metal and ligand ions

where the first multiplier is the projection operator to a ferromagnetic (spin-triplet) state of a dimer M_1M_2, and the first term in square brackets is the projection to the orbitals $|3x^2 - r^2\rangle$ and $|3y^2 - r^2\rangle$ at respective sites 1 and 2 and similarly for the second term in the square brackets, with the corresponding exchange of relevant orbitals (Fig. 3a). Here, T_x^z and T_y^z are the operators corresponding to $|3x^2 - r^2\rangle$ and $|3y^2 - r^2\rangle$ orbitals:

$$T_x^z = \frac{1}{2}\tau^z - \frac{\sqrt{3}}{2}\tau^x,$$
$$T_y^z = \frac{1}{2}\tau^z + \frac{\sqrt{3}}{2}\tau^x. \quad (5)$$

Only these orbitals overlap with $|p_x\rangle$ and $|p_y\rangle$ orbitals of oxygens O_a (and "reversed" orbitals $|3y^2 - r^2\rangle$ on the site M_1 and $|3x^2 - r^2\rangle$ on site M_2 with p orbitals of O_b) and contribute to exchange; orthogonal orbitals do not overlap with p orbitals and do not contribute to the exchange (e. g., the $|y^2 - z^2\rangle$ orbital at a site M_1 is orthogonal to all p orbitals of oxygen O_a in Fig. 3a). In effect, the spin exchange turns out to be ferromagnetic for any ordering of e_g orbitals.

This fact is also illustrated in Fig. 3b for $|x^2 - y^2\rangle$ ferro-orbital ordering. This orbital from the site M_1 overlaps with the $|p_x\rangle$ orbital of oxygen O_a (and with the $|p_y\rangle$ orbital of oxygen O_b), whereas the same d orbital of the transition-metal site M_2 overlaps with the orthogonal $|p_y\rangle$ orbital of this oxygen (and with the $|p_x\rangle$ orbital of oxygen O_b). In effect, we have ferromagnetic spin exchange of these two ions, stabilized by the Hund's rule exchange at an oxygen, $J_{H,p}$, when we virtually move two electrons from this oxygen to the transition-metal sites M_1 and M_2, such that the resulting ferromagnetic exchange constant becomes

$$\tilde{J} \sim \frac{t_{pd}^4}{\Delta_{CT}^2(\Delta_{CT} + U_p/2)}\frac{J_{H,p}}{(\Delta_{CT} + U_p/2)}, \quad (6)$$

where t_{pd} is the metal–oxygen p–d hopping amplitude, Δ_{CT} is the charge-transfer energy needed to move an electron from an oxygen to a metal ion, $d^n p^6 \rightarrow d^{n+1} p^5$, and U_p is the on-site Coulomb repulsion energy of p electrons at an oxygen site. Such a situation occurs, for instance, in Mn_3O_4 spinel, with Mn^{3+} ion at octahedral sites: the B–B exchange is here ferromagnetic, despite the ferro-orbital ordering (in this case, the occupied e_g orbitals are $|3z^2 - r^2\rangle$ with the corresponding strong tetragonal elongation with $c/a \sim 1.15$). We note that this result is valid for Mott–Hubbard insulators, and it should be modified for the charge-transfer insulators [16] (see, e. g., [14, 17]).

We also note that for t_{2g} electrons with $90°$ M–O–M bonds in contrast to the e_g case, we can have both
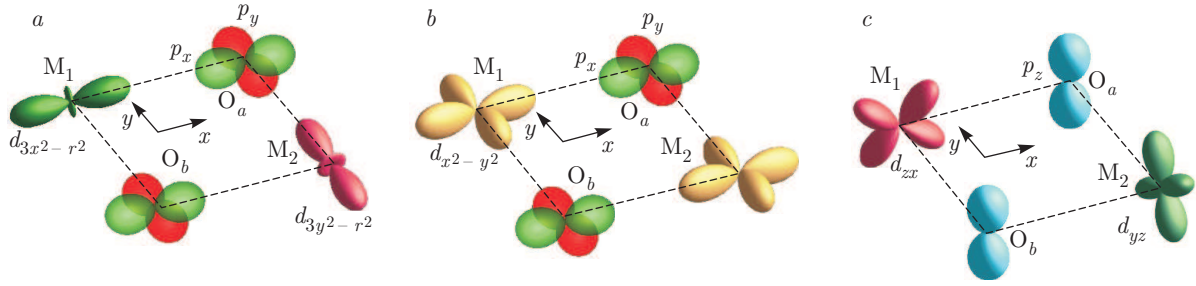
Fig. 3. (*a*) "Active" orbitals contributing to the M$_1$–O$_a$–M$_2$ superexchange for the $90°$ metal–oxygen–metal bonds typical for the common edge geometry. (*b*) Ferro-orbital ordering of $|x^2 - y^2\rangle$ orbitals in the xy plane in the case of edge-sharing octahedra. (*c*) Antiferro-orbital ordering of $|yz\rangle$ and $|zx\rangle$ orbitals in the xy plane in the case of edge-sharing octahedra

ferro- and antiferromagnetic exchange, depending on the orbital occupation and on the exchange path. For antiferro-orbital ordering with orbitals shown in Fig. 3c (occupied orbitals are $|zx\rangle$ and $|yz\rangle$ on the M$_2$O$_2$ plaquette in the xy plane), the overlap with the $|p_z\rangle$ orbital of the oxygen O$_a$ gives strong antiferromagnetic spin exchange with

$$\tilde{J} \sim \frac{t_{pd}^4}{\Delta_{CT}^2} \left[\frac{1}{U} + \frac{1}{\Delta_{CT} + U_p/2} \right]. \qquad (7)$$

For a different orbital occupation, however, the exchange could again be ferromagnetic (see, e. g., Ref. [5, 18] for details).

We also note that in the case of $90°$ M–O–M bonds, the direct d–d hopping amplitude t_{dd}, for example, for the $|xy\rangle$ orbitals lying in the xy plane in Fig. 3c and pointing directly toward one another (along the diagonal on the M$_2$O$_2$ plaquette), may be quite significant and give a contribution to the antiferromagnetic exchange J of about t_{dd}^2/U.

The situation with a common edge is also much richer and more complicated than that with a common corner in the case of strong spin–orbit coupling. Again, as we discussed above, the nontrivial effects appear for partially filled t_{2g} shells, and we have to consider separately the cases with a less than-half-filled t_{2g} shell $n_{t_{2g}} < 3$, and a more-than-half-filled shell $n_{t_{2g}} > 3$. As mentioned above, in the first case, we have an inverted multiplet order, with the multiplet with the maximum j (and maximum degeneracy) lying lower in energy. This case is more difficult to consider technically, but at present it also attracts less attention, even though one might expect some interesting properties in this case as well. However, the main attention is attracted nowadays to the second case, e. g., to the systems with Ir^{4+}, Ru^{3+} (d^5), and Ir^{5+}, Ru^{4+} (d^4), where the ground state of an isolated ion is the state with the minimum

$j = 1/2$ for d^5 and the nonmagnetic $j = 0$ state for the d^4 configuration. How good is the limit of isolated ions for concentrated systems, in which the intersite electron hopping may become comparable to or even exceed the spin–orbit coupling, is a very important and open question. However, if the atomic limit could be used as a valid starting point and the electron hopping be treated as a small perturbation, one would obtain a very nontrivial result for d^5 ions (like Ir^{4+}) in the common edge geometry: the resulting exchange projected to $j = 1/2$ states has not a Heisenberg, but rather an Ising form [14] of the type of $\sigma^z \sigma^z$, where the z axis is the direction perpendicular to the plane of the M$_2$O$_2$ (e. g., Ir$_2$O$_2$) plaquette. For systems with honeycomb lattices like Na$_2$IrO$_3$ [19] or RuCl$_3$ [20], the resulting exchange contains different effective spin combinations ($\sigma^x \sigma^x$, $\sigma^y \sigma^y$, and $\sigma^z \sigma^z$) for different bonds, and hence in effect these compounds may be an example of what is known as system with the Kitaev interaction [21] — a particular case of the so-called compass model [4] (see also [22]). From our perspective, we again see that strong spin–orbit coupling acts against the usual (Jahn–Teller) orbital ordering, reducing initial degeneracy of the system differently than the usual orbital ordering does.

4. SPIN–ORBITAL EXCHANGE FOR THE OCTAHEDRA WITH A COMMON FACE

Both situations, with MO$_6$ octahedra with common corners (one common ligand, $\sim 180°$ M–O–M bonds) and with a common edge (two common oxygens, $\sim 90°$ M–O–M bonds) are rather well studied theoretically and are considered in many publications (see, e. g., [1, 4, 5, 18]). However, there exists a third, much less studied situation with neighboring MO$_6$ octahedra having a common face, i. e., having three common
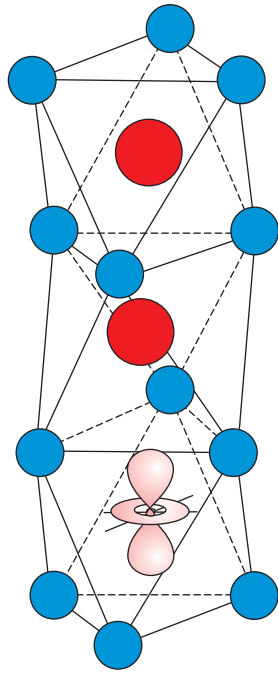
Fig. 4. A chain of face-sharing octahedra. Large and small circles respectively denote metal and ligand ions. The a_{1g} orbital, which has a strong direct overlap with a similar orbital on the neighboring site, is shown for one transition metal ion

oxygens. This situation is illustrated schematically in Fig. 4. Here, the superexchange occurs via three oxygens, with the M–O–M angle for ideal (undistorted) MO_6 octahedra equal to about $70.5°$. In this case (as well as in the case of edge-sharing octahedra, see Fig. 2) the direct d–d hopping can be rather large (the metal–metal distance in Figs. 2 and 4 is usually rather short, sometimes even shorter than that distance in the corresponding metal!); for a common face, the corresponding orbital of a_{1g} symmetry has a form shown for one transition-metal ion in Fig. 4. The situation with the orbital ordering and the form of the resulting spin and orbital exchange for compounds with face-sharing octahedra was not known until recently. Nevertheless, experimentally there are many transition-metal compounds with such a geometry. These are, for example, hexagonal crystals like $BaCoO_3$ [23], $CsCuCl_3$ [24], or $Ba_9Rh_8O_{24}$ [25] (see the right part of Fig. 5, containing infinite columns of face-sharing ML_6 octahedra, where L stands for ligands O, Cl,. . .). Many other similar systems have finite face-sharing blocks, e. g., $Ba_5AlIr_2O_{11}$ [26], $BaIrO_3$ [27], or $BaRuO_3$ [28, 29], $Ba_3CuSb_2O_9$ [30]. There can exist more complicated connections of such blocks, like in $Ba_4Ru_3O_{10}$ [31] (the middle part of Fig. 5). Such systems have very diverse properties: some of them are metallic, but there are also good insulators among them, with very different magnetic properties. Anyway, the first problem to consider for such systems is the question of a possible orbital and magnetic exchange in this geometry. This question was recently addressed in [7]; below, we, first, briefly reproduce these results, and then generalize them to certain specific situations, in particular, to the case of different distortions of octahedra and to the strong spin–orbit coupling.

We consider the form of the spin–orbital ("Kugel–Khomskii") superexchange for transition metals with double or triple orbital degeneracy for neighboring transition-metal ions with face-sharing octahedra. One surprising result of our study is that, whereas the form of orbital term in Hamiltonian (1) is rather complicated for a doubly degenerate system of perovskite type with $180°$ M–O–M bonds [4], a situation similar to the symmetric model in Eq. (2) is realized for a common face. In effect, in such real systems, the dominant term proportional to t^2/U in the spin–orbital superexchange has a very high symmetry, SU(4), and therefore such materials may be real examples of the applicability of such a fancy model (the higher-order terms in this Hamiltonian, containing Hund's rule coupling, J_H/U or J_H/Δ_{CT} [16], have a more complicated form; see below).

The MO_6 octahedra often have trigonal distortions in such geometry (e. g., they are elongated or compressed along the vertical z axis connecting transition-metal ions in the chain). Such local distortions lead to the splitting of t_{2g} orbitals into the a_{1g} singlet and the e_g^π doublet, Fig. 6b; the original e_g (e_g^σ) doublet remains unsplit. Also the crystal structure itself leads to such a trigonal crystal field splitting even for ideal undistorted MO_6 octahedra, in particular, due to interactions with the transition metal ions in neighboring octahedra. It can be shown that if we have a partially filled e_g^π doublet, the resulting superexchange is very similar to that for "real" e_g electrons. Nevertheless, there is one important difference when we are dealing with t_{2g} states, in contrast to e_g ones: for e_g states, the orbital momentum is quenched and the real relativistic spin–orbit coupling $\lambda \mathbf{l} \cdot \mathbf{S}$ does not work in the first order, but for t_{2g} electrons it is not the case, and the spin–orbit coupling has to be taken into account. It can modify the resulting form of superexchange even when spin–orbit coupling is relatively weak. The effect of spin–orbit coupling can be especially important for heavy $4d$ and especially $5d$ elements, for which λ may be comparable with the Hund's rule coupling constant J_H and even with the Hubbard interaction U. In this

Ba$_5$AlIr$_2$O$_{11}$ Ba$_4$Ru$_3$O$_{10}$ Ba$_9$Rh$_8$O$_{24}$
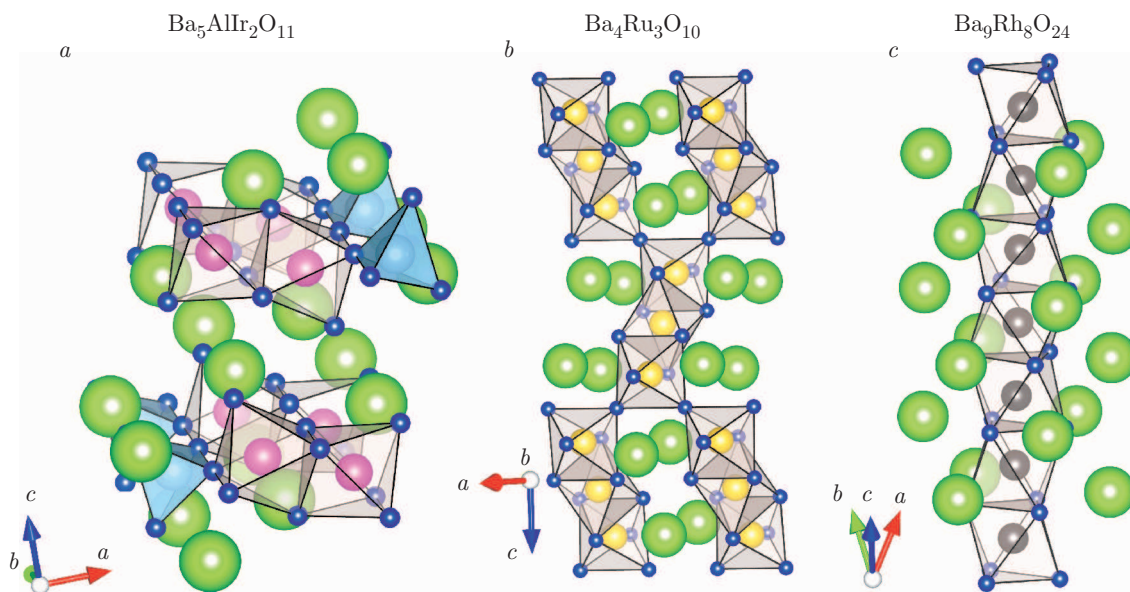
Fig. 5. (Color online) Different arrays of face-sharing octahedra in various transition metal compounds
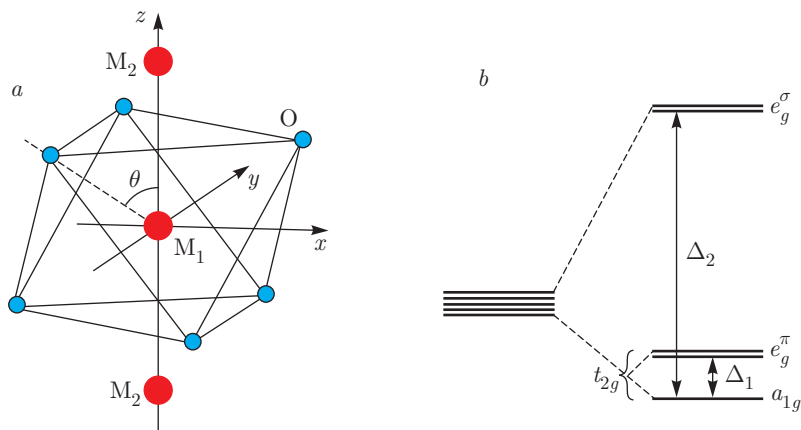
Fig. 6. (a) Magnetic atom (M) surrounded by a trigonally distorted oxygen (O) octahedron in transition metal compounds with face sharing. Distortions are determined by the angle θ; the value $\cos\theta_0 = 1/\sqrt{3}$ corresponds to an undistorted octahedron. Magnetic atoms often form a quasi-one-dimensional chain directed along the z axis. (b) Crystal field splitting of d orbitals of the magnetic atom. The splitting of t_{2g} levels (Δ_1) is due to both the trigonal distortions of oxygen octahedra and the contribution from the neighboring M atoms to the crystal field. The sign of Δ_1 can be different depending on the type of distortions

case, we may again need to go over to the description in terms of the effective total momentum $\mathbf{j} = \mathbf{l} + \mathbf{S}$. As mentioned in Sec. 2, for Ir^{4+} (t_{2g}^5), for example, the resulting picture corresponds to the doublet $j = 1/2$.

The form of the resulting exchange for these effective Kramers doublets $j = 1/2$ in the cases of a common corner and a common edge was presented in Secs. 2 and 3. How this interaction would look for the face-sharing octahedra, e. g., in BaIrO$_3$, was not studied yet; we consider this case, too, and derive the corresponding form of the superexchange. It turns out that for the face-sharing octahedra, the form of the exchange for this

doublet is again more symmetric and has the Heisenberg form $\boldsymbol{\sigma}_i \cdot \boldsymbol{\sigma}_j$, i. e., it resembles the case of the 180° Ir–O–Ir bonds.

4.1. The model

We consider a linear chain of $3d$ ions located at the centers of anion octahedra with face-sharing geometry. Two reference systems are of interest: the local tetragonal reference system of each magnetic ion and a global trigonal system in which the z axis is directed along the chain and the x and y axes are in the plane perpendi-

cular to the chain. We note that two nearest-neighbor ions have relatively rotated local axes and therefore we cannot use the same tetragonal reference system for them. The local tetragonal reference systems are chosen such that the trigonal z axis corresponds to the same [111] direction for them. In what follows, we choose the trigonal reference frame as shown in Fig. 6a. The trigonal distortions can be characterized by the angle θ also shown in this figure. For the ideal MO_6 octahedron, we have $\theta = \theta_0 \equiv \arccos(1/\sqrt{3}) = 54.74°$, while the M–O–M angle is $\beta_0 = \pi - 2\theta_0 \approx 70.5°$.

The crystal field felt by the magnetic ions has an important component of cubic symmetry due to the octahedra of anions, and also a component with trigonal symmetry due to both the ions along the chain and the trigonal distortions of octahedra. In an octahedral field, the electron d levels are split into a triple-degenerate level (t_{2g}) and a doubly degenerate level (e_g). These levels can be further split by the trigonal field and the spin–orbit coupling. We study these cases separately.

4.2. Undistorted octahedra, e_g levels

As a minimum model for the chain, we take the Hubbard model for degenerate electrons, in which we also make a simplifying assumption that the on-site Hubbard repulsion U is the same for all orbitals (i. e., we effectively put the Hund's rule coupling J_H to zero). This simplification is sufficient for our main purposes; we mention possible modifications due to the inclusion of J_H when necessary. This Hamiltonian has the form

$$H = \sum_{\langle ij \rangle} \sum_{\gamma\gamma'} \sum_{\sigma\sigma'} t_{ij}^{\gamma\gamma'} c_{i\gamma\sigma}^{\dagger} c_{j\gamma'\sigma'} +$$
$$+ \frac{U}{2} \sum_i \sum_{\gamma\gamma'} \sum_{\sigma\sigma'} n_{i\gamma\sigma} n_{i\gamma'\sigma'} (1 - \delta_{\gamma\gamma'}\delta_{\sigma\sigma'}), \quad (8)$$

$c_{i\gamma\sigma}^{\dagger}$ and $c_{i\gamma\sigma}$ are the creation and annihilation operators of a d electron with the orbital state γ and spin projection σ located at site i, $n_{i\gamma\sigma} = c_{i\gamma\sigma}^{\dagger} c_{i\gamma\sigma}$, and $\langle ij \rangle$ denotes the summation over nearest-neighbor sites. The first term describes the kinetic energy and the second one corresponds to the on-site Coulomb repulsion, which we treat as the largest parameter (i. e., we consider the case of strong Mott insulators with orbital degeneracy). As is shown below, the situation where the effective d–d hopping occurs via ligands (in this case, via three oxygens, see Fig. 6a) can also be reduced to this form.

We first consider the chain build up by the ideal metal–oxygen octahedra. We start with calculating the orbitals of interest at each site. It is known (see, e. g., Ref. [13]) that both the trigonal field and the spin–orbit coupling do not split the e_g levels. In the trigonal coordinate system, the e_g doublet for two neighboring magnetic ions along the chain can be written as [7, 32]

$$|d_1\rangle = \frac{1}{\sqrt{3}}|x^2 - y^2\rangle - \sqrt{\frac{2}{3}}|xz\rangle,$$
$$|e_1\rangle = -\frac{1}{\sqrt{3}}|xy\rangle - \sqrt{\frac{2}{3}}|yz\rangle \quad (9)$$

for an ion M_1 and

$$|d_2\rangle = \frac{1}{\sqrt{3}}|x^2 - y^2\rangle + \sqrt{\frac{2}{3}}|xz\rangle,$$
$$|e_2\rangle = -\frac{1}{\sqrt{3}}|xy\rangle + \sqrt{\frac{2}{3}}|yz\rangle \quad (10)$$

for the nearest-neighbor ion M_2.

Electron hopping amplitudes entering Hamiltonian (8) have two contributions in our case, which can be of the same order of magnitude for this particular geometry: the direct hopping between two magnetic ions along the chain, $t_{\gamma\gamma'}^{d-d}$, and the indirect (superexchange) hopping via the anions, $t_{\gamma\gamma'}^{via\,A}$. We consider both situations separately.

It is easy to see that the direct d–d hopping exists only between the same orbitals. The corresponding hopping integrals can be expressed through the Slater–Koster parameters [33]

$$\langle xy|\hat{t}|xy\rangle = \langle x^2 - y^2|\hat{t}|x^2 - y^2\rangle = V_{dd\delta}, \quad (11)$$

$$\langle yz|\hat{t}|yz\rangle = \langle xz|\hat{t}|xz\rangle = V_{dd\pi}. \quad (12)$$

Hence, in effect, we have only diagonal (and equal) hoppings

$$t^{d-d} = t_{|d_2\rangle|d_1\rangle}^{d-d} = t_{|e_2\rangle|e_1\rangle}^{d-d} = \frac{1}{3}V_{dd\delta} + \frac{2}{3}V_{dd\pi} \quad (13)$$

and

$$t_{|e_2\rangle|d_1\rangle}^{d-d} = t_{|e_2\rangle|d_1\rangle}^{d-d} = 0. \quad (14)$$

Similarly, it can be shown that the hopping integrals via intermediate oxygen ions, after we sum over all three of them, have the same feature [7],

$$t_{\gamma\gamma'}^{via\,A} = t = t_0\delta_{\gamma\gamma'}, \quad t_0 = \frac{3}{2}(t_1 + t_2), \quad (15)$$

where $t_1 = \langle d_1|\hat{t}^{via\,O}|d_2\rangle$ and $t_2 = \langle e_1|\hat{t}^{via\,O}|e_2\rangle$ are the hopping integrals via one of the oxygen ions. As a result, we here have exactly the same situation as in the symmetric model described in Sec. 2, with the hopping between two degenerate orbitals satisfying the

relations $t_{11} = t_{22} = t$ and $t_{12} = 0$, and therefore, in the leading approximation, we actually have SU(4) spin–orbital model (2) also in the case of face-sharing transition metal compounds.

This is a rather general result based only on the existence of the three-fold trigonal axis and it does not depend on the specific features of the superexchange paths.

When going beyond the lowest order and including the Hund's rule coupling J_H, the total exchange takes the form (see also [4])

$$
\begin{aligned}
H_{eff} = \frac{t^2}{U} \sum_{\langle ij \rangle} \Bigg\{ & \left(\frac{1}{2} + \mathbf{S}_i \cdot \mathbf{S}_j \right) \left(\frac{1}{2} + \boldsymbol{\tau}_i \cdot \boldsymbol{\tau}_j \right) + \\
+ \frac{J_H/U}{1 - (J_H/U)^2} & \left[2 \left(\boldsymbol{\tau}_i \cdot \boldsymbol{\tau}_j - \tau_i^z \tau_j^z \right) - \left(\frac{1}{2} + 2\mathbf{S}_i \cdot \mathbf{S}_j \right) \times \right. \\
\times & \left. \left(\frac{1}{2} - 2\tau_i^z \tau_j^z \right) \right] + \frac{(J_H/U)^2}{1 - (J_H/U)^2} \left[- \left(\frac{1}{2} - 2\tau_i^z \tau_j^z \right) + \right. \\
& \left. + 2 \left(\frac{1}{2} + \mathbf{S}_i \cdot \mathbf{S}_j \right) \left(\boldsymbol{\tau}_i \cdot \boldsymbol{\tau}_j - \tau_i^z \tau_j^z \right) \right] \Bigg\}. \quad (16)
\end{aligned}
$$

We note here that, strictly speaking, similarly to the case of a common edge in Sec. 3, Hamiltonian (16) is valid only for Mott–Hubbard insulators, when $U < \Delta_{CT}$. The opposite limit of charge-transfer insulators, $U > \Delta_{CT}$, requires separate analysis.

4.3. Undistorted octahedra, the t_{2g} case

The systems with transition-metal ions surrounded by octahedra with a common face typically have the trigonal symmetry, even for regular MO_6 octahedra. In reality, however, these octahedra are also usually distorted. Such distortions could preserve the C_3 symmetry and would correspond to a compression or stretching of these octahedra along the z direction shown in Fig. 6a. The trigonal crystal field does not split the e_g levels, but leads to a splitting of the t_{2g} levels into an a_{1g} singlet and an e_g^π doublet. Which level lies lower, singlet or doublet, depends on the sign of the trigonal crystal field. In the trigonal coordinate system (with the z axis along the chain), these wave functions are as follows: for the a_{1g} singlet,

$$
|a_1\rangle = |3z^2 - r^2\rangle, \quad (17)
$$

and for the e_g^π doublet,

$$
\begin{aligned}
|b_1\rangle &= -\frac{2}{\sqrt{6}}|xy\rangle + \frac{1}{\sqrt{3}}|yz\rangle, \\
|c_1\rangle &= \frac{2}{\sqrt{6}}|x^2 - y^2\rangle + \frac{1}{\sqrt{3}}|xz\rangle
\end{aligned} \quad (18)
$$

for an ion M_1, and the same singlet

$$
|a_2\rangle = |3z^2 - r^2\rangle \quad (19)
$$

and a doublet

$$
\begin{aligned}
|b_2\rangle &= -\frac{2}{\sqrt{6}}|xy\rangle - \frac{1}{\sqrt{3}}|yz\rangle, \\
|c_2\rangle &= \frac{2}{\sqrt{6}}|x^2 - y^2\rangle - \frac{1}{\sqrt{3}}|xz\rangle
\end{aligned} \quad (20)
$$

for the nearest-neighbor ion M_2.

These expressions are valid for the ideal MO_6 octahedra, where the M–O–M angle is about $70.5°$. The trigonal distortions lead to modifications of the e_g^π wave functions. A detailed description of such modifications is given in the Appendix. These modifications, however, do not change the main conclusion that here too, only diagonal hoppings are nonzero (see below).

If one electron occupies the a_{1g} level, there remains no orbital degeneracy, and the spin exchange is trivially antiferromagnetic. More interesting is the case of one electron (or hole) at the e_g^π level. It can be shown [7] that in this case, similar to the case of "real" e_g electrons discussed in Sec. 4.2, we have a symmetric model with the hoppings $\langle b_1|\hat{t}|b_2\rangle = \langle c_1|\hat{t}|c_2\rangle = t$ and $\langle b_1|\hat{t}|c_2\rangle = 0$, and hence we also eventually have the resulting spin–orbital model (2) with the SU(4) symmetry, or the more general exchange (16). The detailed form of wave functions $|b\rangle$ and $|c\rangle$ depends on the noncubic (here, trigonal) crystal field, and it is different from those written above (see the Appendix), but it does not change conclusions qualitative and only changes numerical values of exchange constants in Hamiltonians (2) and (16).

4.4. Role of spin–orbital interaction

In Secs. 2 and 3, we already presented the form of the effective exchange interaction in the case of a very strong spin–orbit coupling, for which (e. g., for ions like Ir^{4+} or Ru^{3+} with the d^5 configuration) the whole description can sometimes be reduced to that of a separate $j = 1/2$ Kramers doublet (see the E_3 doublet in Fig. 7). In this subsection, we consider the same problem for systems with common faces, also taking trigonal crystal field mentioned in the previous section into account.

First, we consider the simplest case of regular octahedra with the degenerate t_{2g} orbital triplet in same case of ions like Ir^{4+} for a strong spin–orbit coupling. In this case, the wave functions of the separate $j = 1/2$
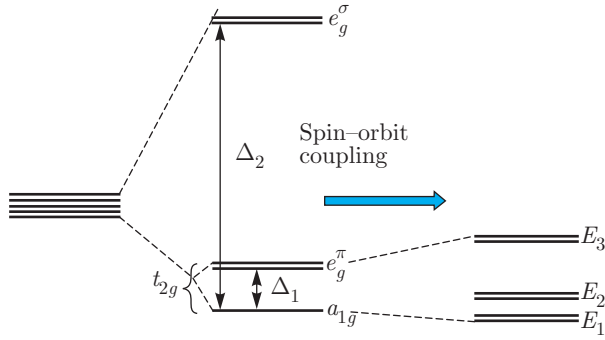
Fig. 7. Spin–orbital interaction splits the e_g^π and a_{1g} energy levels into three Kramers doublets with energies E_1, E_2, and E_3. For undistorted octahedra and negligible effect of nearest-neighbor magnetic atoms, there is one quartet with energy $E_1 = E_2 = -\lambda/2$ and one doublet with energy $E_3 = 2\lambda$

doublet E_3 for the site M_1 are analogous to those discussed in [5, 13, 14]:

$$\begin{aligned}
|j = +1/2\rangle &= \frac{1}{\sqrt{3}}\left[-|a_{1g}, \uparrow\rangle + |(-c_1 + ib_1), \downarrow\rangle\right], \\
|j = -1/2\rangle &= \frac{1}{\sqrt{3}}\left[-|a_{1g}, \downarrow\rangle + |(c_1 + ib_1), \uparrow\rangle\right],
\end{aligned} \tag{21}$$

and a similar expression for the site M_2 with the wave functions $|b_2\rangle$ and $|c_2\rangle$ instead of $|b_1\rangle$ and $|c_1\rangle$ (see (17)–(20)). Here, a_{1g} states correspond to $l_{eff}^z = 0$, and the states $|b_1 \pm ic_1\rangle$ to states with $l_{eff}^z = \pm 1$ for quantization along the z axis in the global coordinate system of Fig. 6a.

Projecting into this manifold and using wave functions (17)–(20), we easily obtain that the hopping matrix elements are diagonal and equal to each other both for direct d–d hopping and for hopping via oxygens,

$$\begin{aligned}
\langle 1/2|\hat{t}|1/2\rangle &= \langle -1/2|\hat{t}| - 1/2\rangle = t, \\
\langle 1/2|\hat{t}| - 1/2\rangle &= 0.
\end{aligned} \tag{22}$$

Similarly to the case in Sec. 2, we immediately see that the exchange written in terms of the effective spin $1/2$ of the $j = 1/2$ doublet again takes the form of Heisenberg interaction (3).

We now consider which modifications we can expect in the case of trigonal splitting of t_{2g} states, and also of other electron occupations. We note that the treatment below deals with one-electron levels, i.e., effectively corresponds not to the Russel–Sounders, but to the JJ coupling. This is actually the assumption implicitly made in most treatments of systems with strong spin–orbit coupling like iridates, although it is not always stated explicitly.

As mentioned above, for systems with a common face, the trigonal splitting of t_{2g} levels is very typical. The detailed treatment of this situation is given in the Appendix. Here, we summarize and qualitatively explain the main findings. As can be shown, inclusion of both (strong) spin–orbit coupling and the trigonal crystal field leads to the structure of levels shown in Fig. 7. Typically, except at some isolated points in a parameter space, the t_{2g} levels are split into three Kramers doublets (for the cubic crystal field, the doublets E_1 and E_2 in Fig. 7 are degenerate and combine into a $j = 3/2$ quartet). For example, if we have a system like Ir^{4+} (d^5), we have one electron at the E_3 doublet. In general, wave functions (21) of this doublet would be different from those of unsplit t_{2g} triplets. Nevertheless, at least for the large t_{2g}–e_g splitting $10Dq$ (ignoring a possible admixture of "real" e_g states), these are all composed of a superposition of t_{2g} functions (17)–(20) or of functions with $|l_z = 0\rangle = |a_{1g}\rangle$ and $|l^z = \pm 1\rangle = (1/\sqrt{2})|b_{1,2} \pm ic_{1,2}\rangle$ in the form

$$\begin{aligned}
|+\rangle &= c_0|l^z = 0, \uparrow\rangle + c_1|l^z = |+1, \downarrow\rangle, \\
|-\rangle &= c_0|l^z = 0, \downarrow\rangle + c_{-1}|l^z = |-1, \uparrow\rangle
\end{aligned} \tag{23}$$

with $c_1 = c_{-1}$ and $c_0^2 + c_1^2 = 1$. Again, in the general case, when we take into account that hopping matrix elements are nonzero only for diagonal hopping, $\langle 0|\hat{t}|0\rangle = t_0$, $\langle +|\hat{t}|+\rangle = \langle -|\hat{t}|-\rangle = t_1$, and nondiagonal hoppings are zero, $\langle 0|\hat{t}| \pm 1\rangle = \langle +|\hat{t}|-\rangle = 0$, we finally obtain that also in this general case, we have the same symmetric situation, with $\langle +|\hat{t}|+\rangle = \langle -|\hat{t}|-\rangle = t$, $\langle +|\hat{t}|-\rangle = 0$, i.e., we have only a diagonal and equal hopping within the E_3 doublet.

Consequently, in this case in general, in the leading approximation, we obtain simple Heisenberg interaction (3) for this Kramers doublet (if indeed spin–orbit coupling is strong enough for this doublet to be well separated from the E_1 and E_2 levels). This can be traced back to the fact that electron hopping, on the one hand, preserves spin, $t_{\uparrow,\uparrow} = t_{\downarrow,\downarrow} = t$, $t_{\uparrow,\downarrow} = 0$, but also conserves the orbital momentum, and hence that $\langle 0|\hat{t}|0\rangle$, $\langle +1|\hat{t}| + 1\rangle$, and $\langle -1|\hat{t}| - 1\rangle$ are nonzero, but hoppings with a change of the orbital momentum disappear, i.e., nondiagonal matrix elements are zero. This in effect is responsible for the realization of the symmetric model, which finally gives the Heisenberg interaction for very strong spin–orbit coupling (an isolated doublet E_3). However, in the general situation, for an arbitrary relation between the spin–orbit coupling and the crystal field splitting and for other signs of this trigonal crystal field and other filling of d levels, the situation can be very different and may require spe-

cial treatment (some basis for which is presented in the Appendix).

5. CONCLUSIONS

In this paper, we presented a survey of the spin–orbital interaction for orbitally degenerate Mott insulators for different local geometries (MO_6 octahedra with a common corner, a common edge, or a common face), paying main attention to the "third case" of the common face, which, strangely enough, was practically not considered in the existing literature. The main message is that the general form and the details of the spin–orbital ("Kugel–Khomskii") exchange interaction very strongly depends on this local geometry, and therefore the commonly accepted paradigm (ferro-orbitals $\leftrightarrow$ antiferro-spins, and vice versa, antiferro-orbitals $\leftrightarrow$ ferro-spins), derived for $180°$ degree metal–oxygen–metal bonds (common corner), is not valid in general.

Rather surprisingly, the "third case" of octahedra with a common face turns out to be in some sense simpler and more symmetric than the other two situations, despite the apparently more complicated local geometry (exchange via three oxygens, with a "not simple" M–O–M angle about $70°$, etc.). In particular, for doubly degenerate case (e_g orbitals or an e_g^π doublet produced out of a t_{2g} triplet by trigonal splitting, typical for this case) the effective spin–orbital model has a highly symmetric form (2), i. e., it contains scalar products of both spin operators $\mathbf{S}$ and orbital operators $\boldsymbol{\tau}$ describing the orbital doublet. The resulting exchange (2) has not only the $SU(2) \times SU(2)$ symmetry dictated by these scalar products, but they also enter with coefficients such that the resulting symmetry is even much higher, $SU(4)$, yielding a very nice theoretical model, which for example is exactly solvable in the 1D case, etc.

Thus, the materials with MO_6 octahedra sharing a face can be good model systems for studying possible manifestations of this high symmetry. Similarly, local geometry largely determines the resulting form of the exchange in case of a very strong spin–orbit coupling $\lambda\mathbf{L} \cdot \mathbf{S}$ — the situation typical for $4d$ and $5d$ systems. As is already known, for example, for ions with the d^5 configuration, such as the currently popular Ir^{4+}, the exchange Hamiltonian for the lowest Kramers doublet $j = 1/2$ has the Heisenberg form for $180°$ M–O–M bonds (common corner), but it is a highly anisotropic (locally Ising) interaction for $90°$ bonds (common edge). Again, the situation for sys-

tems with a common face turns out to be simpler in the case of strong spin–orbit coupling. The exchange for Kramers doublets $j = 1/2$ again has the Heisenberg form, $H \sim J\sum \boldsymbol{\sigma}_i \cdot \boldsymbol{\sigma}_j$, where $\boldsymbol{\sigma}$ is the effective spin describing the $j = 1/2$ doublet.

We have also shown that the account taken of the trigonal splitting, very typical of the case of a common face, does not change the situation qualitatively, although definite quantitative changes appear.

These situations considered above, although the most typical ones, do not exhaust all the variety of local geometries met in transition metal compounds. For example, transition-metal ions can be not in O_6 octahedra but, for example, in O_4 tetrahedra, like A sites in spinels or Co ions in $YBaCo_4O_7$. Or they may be in trigonal bipyramids (Mn in $YMnO_3$) or in prisms (half of Co ions in $Ca_3Co_2O_6$), etc. Every such case requires special treatment, one cannot uncritically transfer the know-how acquired in considering the spin–orbit system, say, in perovskites to these cases. An important conclusion is that this concerns not only these, more complicated cases but also the situation with more conventional materials containing transition-metal ions in O_6 octahedra, which may be more complicated than is usually assumed. Apart from the specific results for the "third case" of octahedra sharing a face, this warning is the main message of this paper.

APPENDIX

Effects of trigonal distortions

1. Face-sharing geometry with trigonal distortions. Wave functions and energy levels

Actually, we never deal with ideal octahedra. In particular, the chain of face-sharing octahedra is usu-

ally stretched or compressed. The effect of such distortions can be described in terms of the crystal field of trigonal symmetry. Below, in Part 1, for completeness, we briefly reproduce and extend the results of the treatment of trigonal splitting in Ref. [7]; these results are important for us for the general treatment of the effect of the spin–orbit coupling in Part 2 of Appendix.

An elementary building block of the transition metal compounds with face-sharing octahedra is shown in Fig. 6a. Each magnetic atom is surrounded by a distorted oxygen octahedron. Distortions can be described by a single parameter θ, which is the angle between the z axis and the line connecting M and O atoms (see Fig. 6a). For an undistorted octahedron, we have $\theta = \theta_0 = \arccos(1/\sqrt{3})$. The crystal field splits 5-fold degenerate d electron levels of the transition metal atom into two doubly degenerate e_g^σ, e_g^π levels, and an a_{1g} level, like shown above in Fig. 6b. The energy difference Δ_1 between the e_g^π and a_{1g} levels can be positive or negative depending on the type of trigonal distortions and other parameters of the system.

We should find the wave functions of the e_g^σ, e_g^π, and a_{1g} levels in the case of distorted octahedra. We first neglect the contribution to the crystal field from neighboring magnetic cations. In the point-charge approximation, the crystal field potential acting onto a chosen cation located at a point $\mathbf{r}$ can be represented as a sum of Coulomb terms

$$V(\mathbf{r}) = v_0 \sum_i \frac{r_0}{|\mathbf{r} - \mathbf{r}_i|}, \qquad (A.1)$$

where $\mathbf{r}_i$ are the positions of ligand ions. For d states, the existence of the three-fold symmetry axis leads to a significant simplification of the expression for the crystal field

$$V(\mathbf{r}) = v_0(r) + v_1(r) \sum_{s=1}^{3} P_2(\cos\theta_s) +$$
$$+ v_2(r) \sum_{s=1}^{3} P_4(\cos\theta_s), \quad (A.2)$$

where P_2 and P_4 are the Legendre polynomials,

$$P_2(x) = \frac{1}{2}(3x^2 - 1), \quad P_4(x) = \frac{1}{8}(34x^4 - 30x^2 + 3).$$

Here, we took the symmetry in the arrangement of two opposite edges of the ligand octahedron into account, and as a result we have

$$\cos\theta_s = \cos\theta\cos\theta' + \sin\theta\sin\theta'\cos\left(\phi' - \frac{2\pi s}{3}\right), \quad (A.3)$$

where θ' and ϕ' describe the direction of $\mathbf{r} = r\{\sin\theta'\cos\phi', \sin\theta'\sin\phi', \cos\theta'\}$.

Next, it is necessary to find the matrix elements of the crystal field for the complete set of d functions and to diagonalize the corresponding matrix. This gives us both the wave functions of e_g^σ, e_g^π, and a_{1g} levels and their energies, depending on the trigonal distortions. The details of such calculations can be found in [7]. Choosing the reference frame as is shown in Fig. 6a, we eventually obtain expressions for the wave functions in the forms similar to those discussed above for undistorted octahedra. For the e_g levels (e_g^σ orbitals), we have (cf. Eqs. (9), (10))

$$|d_{1,2}\rangle = \sin\frac{\alpha}{2}|x^2 - y^2\rangle \mp \cos\frac{\alpha}{2}|xz\rangle,$$
$$|e_{1,2}\rangle = -\sin\frac{\alpha}{2}|xy\rangle \mp \cos\frac{\alpha}{2}|yz\rangle. \qquad (A.4)$$

For the t_{2g} orbitals, we have the same a_{1g} singlet, Eqs. (17) and (19), and the e_g^π doublet (cf. with Eqs. (18) and (20)),

$$|b_{1,2}\rangle = -\cos\frac{\alpha}{2}|xy\rangle \pm \sin\frac{\alpha}{2}|yz\rangle,$$
$$|c_{1,2}\rangle = \cos\frac{\alpha}{2}|x^2 - y^2\rangle \pm \sin\frac{\alpha}{2}|xz\rangle. \qquad (A.5)$$

The "$\mp$" and "$\pm$" signs in the above expressions for cation wave functions for neighboring magnetic ions occur since the oxygen octahedra surrounding neighboring metal ions are transformed into each other by the 180° rotation about the z axis. The parameter α in Eqs. (A.4) and (A.5) depends on the trigonal distortions as

$$\cos\alpha = \frac{a}{\sqrt{a^2 + b^2}}, \quad a = a_2 + a_4, \qquad (A.6)$$

where

$$a_4 = -\frac{3}{2}\left(\frac{5}{2}\cos^4\theta - \frac{15}{7}\cos^2\theta + \frac{3}{14}\right),$$
$$a_2 = \frac{27}{35}\kappa\left(3\cos^2\theta - 1\right), \quad b = 3\sin^3\theta\cos\theta. \qquad (A.7)$$

The parameter κ is defined as

$$\kappa = \frac{\displaystyle\int_0^\infty v_1(r)R_d^2(r)r^2\,dr}{\displaystyle\int_0^\infty v_2(r)R_d^2(r)r^2\,dr}. \qquad (A.8)$$

This parameter depends both on the crystal field coefficients $v_{1,2}(r)$ (see expansion (A.2)) and on the radial part of the wave function $R_d(r)$ for d electrons. The

value of κ depends on the material under study. Both semianalytic and *ab initio* calculations done in Ref. [7] give the estimate $\kappa \sim 0.1$–1.

For the ideal octahedron, we have $\alpha = \alpha_0 \equiv \equiv \pi - 2\theta_0 = \arccos(1/3)$. Substituting this value in Eqs. (A.4) and (A.5), we arrive at the results presented in Sec. 4.3. Stretching (compression) of oxygen octahedra tends to make $\alpha < \alpha_0$ ($\alpha > \alpha_0$).

We now analyze the behavior of the e_g^σ, e_g^π, and a_{1g} energy levels under trigonal distortions. Figure 8 shows the dependence of the energies $E_{e_g^\sigma}$, $E_{e_g^\pi}$, and $E_{a_{1g}}$ on the angle θ varying near $\theta_0 \approx 54.74°$ calculated for two different values of κ. For an ideal octahedron, we have $\Delta_1 = E_{e_g^\pi} - E_{a_{1g}} = 0$ for any κ. The sign of Δ_1 depends on both the type of trigonal distortion (stretching for $\theta < \theta_0$ or compression for $\theta > \theta_0$) and the value of κ. When $\kappa \lesssim 0.5$, the stretching (compression) of the octahedron is $\Delta_1 > 0$ ($\Delta_1 < 0$), while for $\kappa \gtrsim 0.5$, the situation is opposite (see Fig. 8*a,b*). We note that we consider only distortions with θ near θ_0, when $\Delta_2 = E_{e_g^\sigma} - E_{a_{1g}} \sim 10Dq \gg |\Delta_1|$. Such a situation corresponds to the experiment for all known compounds. At the same time, the sign of Δ_1 can be different for different systems. For example, $\Delta_1 > 0$ for $BaCoO_3$ with the chains of face-sharing $Co^{4+}O_6$ octahedra [23].

These results were obtained neglecting the effect of neighboring metal atoms in the chain. Taking the contribution to the crystal field from these atoms into account modifies the parameter a_2 as

$$a_2 \to a_2 - \frac{27\kappa}{35} \frac{Z^*}{12\cos^2\theta}, \qquad (A.9)$$

where Z^* is the effective charge (in units of e) of the metal ion. The parameters a_4 and b, as well as relations (A.4)–(A.6) remain the same. The crystal field from neighboring metal atoms tends to increase Δ_1 and the parameter α. The dependence of the e_g^σ, e_g^π, and a_{1g} energies levels calculated for nonzero Z^* is shown in Fig. 8*c*.

The wave functions in Eqs. (A.4) and (A.5) are the generalization of those considered in the previous section to the case of arbitrary trigonal distortion characterized by an angle α. It is quite straightforward to demonstrate that a similar structure of the e_g^σ and e_g^π wave function leads to the same symmetric spin–orbital Hamiltonian (2) with the SU(4) symmetry at any given value of α.
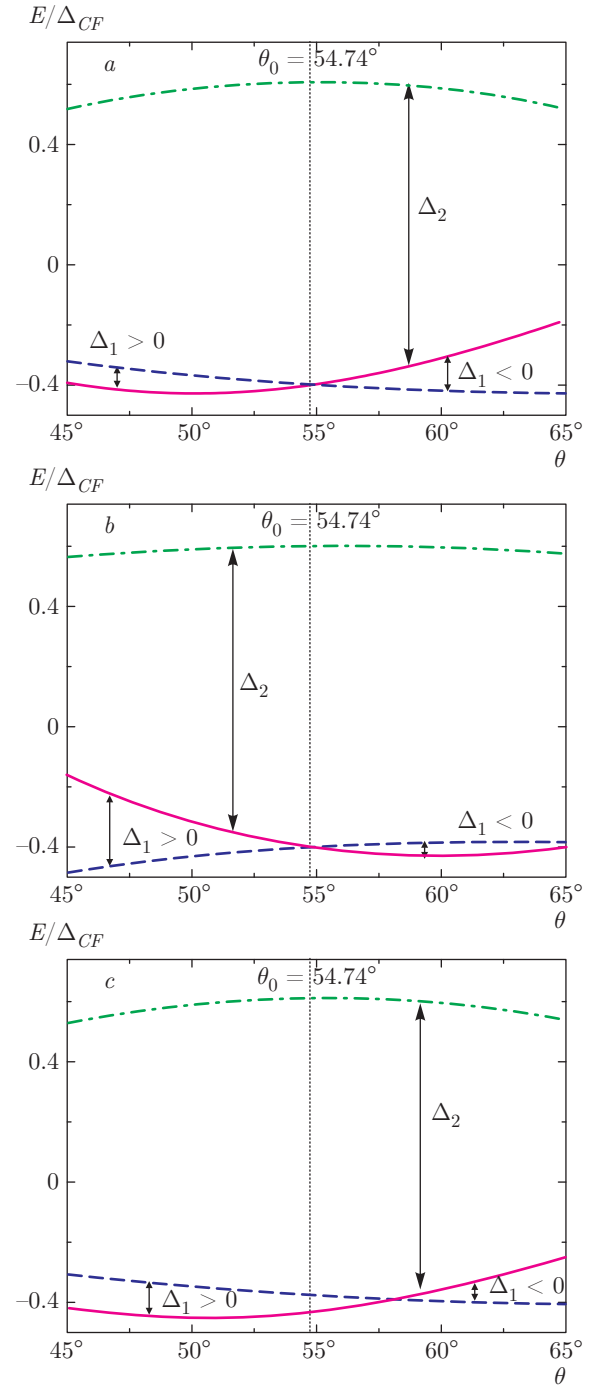
Fig. 8. Energies $E_{a_{1g}}$ (solid line), $E_{e_g^\pi}$ (dashed line), and $E_{e_g^\sigma}$ (dot-dash line) versus the angle θ, calculated for (*a*) $\kappa = 0.1$, $Z^* = 0$, (*b*) $\kappa = 1$, $Z^* = 0$, and (*c*) $\kappa = 0.1$, $Z^* = 3$

2. Spin–orbit coupling in the case of trigonally distorted octahedra

We start from the analysis of the structure of d-electron levels. The spin–orbital interaction Hamil-

tonian has the form

$$H_{SO} = \lambda \mathbf{l} \cdot \mathbf{S}. \qquad (A.10)$$

To find eigenenergies and eigenfunctions of the d-electron levels, we represent the orbital momentum operators l_z and $l_{\pm} = l_x \pm il_y$ in the basis of wave functions $|\mu\rangle$ in which the matrix describing the crystal field splitting is diagonal:

$$\left(\hat{\tilde{l}}_z\right)_{\mu\nu} = \langle\mu| l_z |\nu\rangle, \quad \left(\hat{\tilde{l}}_{\pm}\right)_{\mu\nu} = \langle\mu| l_{\pm} |\nu\rangle. \qquad (A.11)$$

The basic wave functions are

$$|\mu\rangle = \{|e_{g1}^{\sigma}\rangle, |e_{g2}^{\sigma}\rangle, |e_{g1}^{\pi}\rangle, |e_{g2}^{\pi}\rangle, |a_{1g}\rangle\},$$

where

$$\begin{aligned}
|e_{g1}^{\sigma}\rangle &= |d_1\rangle, \quad |e_{g2}^{\sigma}\rangle = |e_1\rangle, \\
|e_{g1}^{\pi}\rangle &= |b_1\rangle, \quad |e_{g2}^{\pi}\rangle = |c_1\rangle
\end{aligned} \qquad (A.12)$$

for a magnetic ion M_1, and

$$\begin{aligned}
|e_{g1}^{\sigma}\rangle &= |d_2\rangle, \quad |e_{g2}^{\sigma}\rangle = |e_2\rangle, \\
|e_{g1}^{\pi}\rangle &= |b_2\rangle, \quad |e_{g2}^{\pi}\rangle = |c_2\rangle,
\end{aligned} \qquad (A.13)$$

for a magnetic ion M_2 (for the definition of $|b_{1,2}\rangle$, $|c_{1,2}\rangle$, $|d_{1,2}\rangle$, and $|e_{1,2}\rangle$, see Eqs. (A.4) and (A.5)). The basic wave function $|a_{1g}\rangle$ is the same for both magnetic ions; it is given by Eq. (17). In this basis, the 5×5 matrix $\hat{V}$ describing the crystal field is diagonal and has the form $\hat{V} = \mathrm{diag}\{\Delta_2, \Delta_2, \Delta_1, \Delta_1, 0\}$. The spin–orbit coupling breaks the degeneracy of d levels with respect to the electron spin. Keeping this in mind, we introduce the second (spin) index to the basic wave functions $|\mu\rangle \rightarrow \rightarrow |\mu, \sigma\rangle$ with $\sigma = \uparrow, \downarrow$. The total Hamiltonian can then be represented in the form of a 10×10 matrix, which can be written in the block-matrix form

$$\hat{H} = \begin{pmatrix} \hat{V} & 0 \\ 0 & \hat{V} \end{pmatrix} + \frac{\lambda}{2} \begin{pmatrix} \hat{\tilde{l}}_z & \hat{\tilde{l}}_- \\ \hat{\tilde{l}}_+ & -\hat{\tilde{l}}_z \end{pmatrix}. \qquad (A.14)$$

Diagonalizing $\hat{H}$ gives the structure of electron levels in the presence of spin–orbit coupling. In the general case, the eigenenergies can be found only numerically. Here, we consider the limit $\Delta_2 \gg \Delta_1, \lambda$, which is realized for a majority of transition metal compounds. In addition, we are interesting in the low-energy sector $|\bar{\mu}, \sigma\rangle = \{|e_{g1}^{\pi}, \sigma\rangle, |e_{g2}^{\pi}, \sigma\rangle, |a_{1g}, \sigma\rangle\}$. The projection of $\hat{H}$ to this reduced basis decreases the rank of the matrix to 6. As a result, we are able to obtain analytic expressions for the eigenenergies and eigenfunctions. There are three doublets with the energies (see Fig. 7)

$$\begin{aligned}
E_1 &= 2(\Delta_1 - \Delta), \\
E_2 &= \Delta - \sqrt{\Delta^2 + \xi^2}, \\
E_3 &= \Delta + \sqrt{\Delta^2 + \xi^2},
\end{aligned} \qquad (A.15)$$

where

$$\Delta = \frac{\Delta_1}{2} + \frac{1 + 3\cos\alpha}{8}\lambda, \quad \xi = \sqrt{\frac{3}{2}}\sin\frac{\alpha}{2}\lambda. \qquad (A.16)$$

The eigenfunctions $|v_{1,2}^{(s)}\rangle$ corresponding to the energies E_s ($s = 1, 2, 3$) are

$$|v_1^{(1)}\rangle = |v_1, \uparrow\rangle, \quad |v_2^{(1)}\rangle = |v_2, \downarrow\rangle, \qquad (A.17)$$

$$\begin{aligned}
|v_1^{(2)}\rangle &= \cos\delta|a_{1g}, \uparrow\rangle + \sin\delta|v_1, \downarrow\rangle, \\
|v_2^{(2)}\rangle &= \cos\delta|a_{1g}, \downarrow\rangle + \sin\delta|v_2, \uparrow\rangle,
\end{aligned} \qquad (A.18)$$

$$\begin{aligned}
|v_1^{(3)}\rangle &= -\sin\delta|a_{1g}, \uparrow\rangle + \cos\delta|v_1, \downarrow\rangle, \\
|v_2^{(3)}\rangle &= -\sin\delta|a_{1g}, \downarrow\rangle + \cos\delta|v_2, \uparrow\rangle,
\end{aligned} \qquad (A.19)$$

where

$$|v_{1,2}, \sigma\rangle = \frac{1}{\sqrt{2}}\left(i|e_{g1}^{\pi}, \sigma\rangle \mp |e_{g2}^{\pi}, \sigma\rangle\right) \qquad (A.20)$$

and

$$\tan 2\delta = \frac{\xi}{\Delta}. \qquad (A.21)$$

We note that while energies of the doublets, E_s, are the same for the M_1 and M_2 magnetic ions, the corresponding eigenfunctions are different due to the $\pm$ signs in Eq. (A.5) defining the eigenfunctions of the e_g^{π} levels. We also note that Eqs. (A.15)–(A.21) were obtained in the limit as $\Delta_2 \rightarrow \infty$. The corrections to this result from the e_g^{σ} sector can be found in the perturbation theory in E_s/Δ_2.

Formulas (A.15)–(A.21) are simplified in the limits of small and large spin–orbit coupling in comparison to the trigonal splitting. In the former case, $\lambda \ll \Delta_1$, we obtain the energy levels up to the first order in λ/Δ_1 as

$$\begin{aligned}
E_1 &\approx \Delta_1 - \frac{1 + 3\cos\alpha}{4}\lambda, \\
E_2 &\approx \Delta_1 + \frac{1 + 3\cos\alpha}{4}\lambda, \quad E_3 \approx 0.
\end{aligned} \qquad (A.22)$$

In the opposite limit $\lambda \gg \Delta_1$, in the leading order, we obtain

$$\begin{aligned}
E_1 &\approx -\frac{1 + 3\cos\alpha}{4}\lambda, \\
E_2 &\approx -\frac{3 - 3\cos\alpha}{4}\lambda, \quad E_3 \approx \lambda.
\end{aligned} \qquad (A.23)$$

In this case, the parameter δ in Eqs. (A.18) and (A.19) is

$$\tan\delta = \sqrt{\frac{3}{2}}\sin\frac{\alpha}{2}. \qquad (A.24)$$

For ideal octahedra and the negligible effect of nearest-neighbor magnetic atoms ($\alpha = \alpha_0 = \arccos(1/3)$,
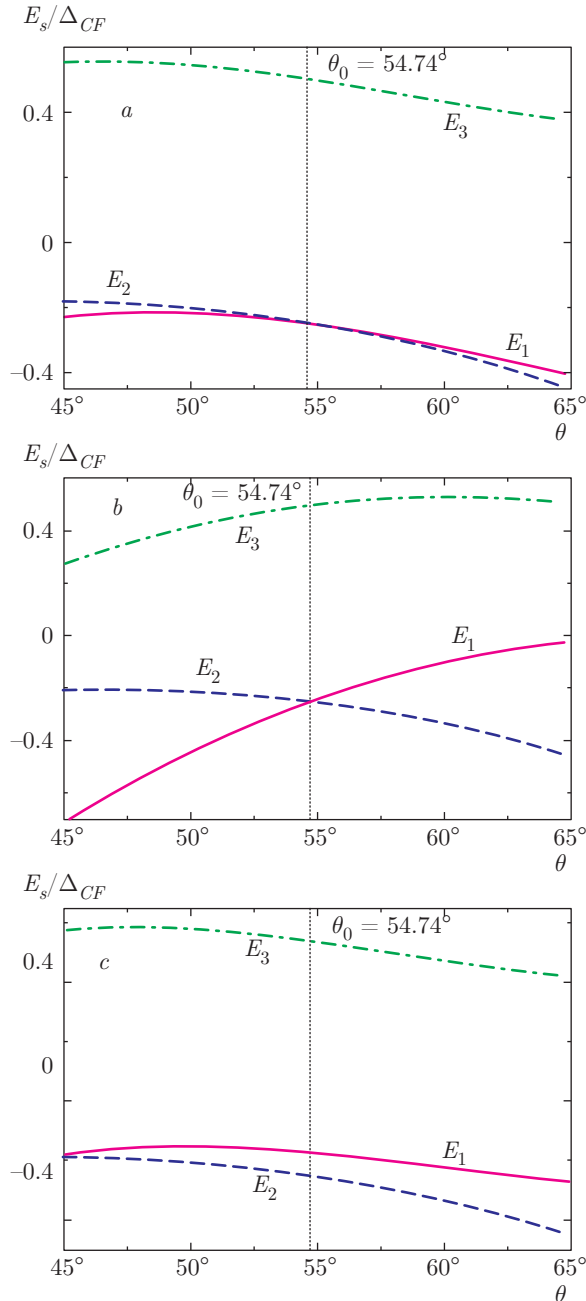
Fig. 9. The energies of the Kramers doublets E_1, E_2, and E_3, as functions of the angle θ calculated for (a) $\kappa = 0.1$, $Z^* = 0$, (b) $\kappa = 1$, $Z^* = 0$, and (c) $\kappa = 0.1$, $Z^* = 3$. For all panels, $\lambda/\Delta_{CF} = 0.5$

$\Delta_1 \equiv 0$), the formulas for E_s and δ are simplified even further:

$$E_1 = E_2 = -\frac{\lambda}{2}, \quad E_3 = \lambda,$$
$$\delta = \arcsin\left(1/\sqrt{3}\right). \tag{A.25}$$

Thus, in this case, we have the low-energy (if $\lambda > 0$) quartet and a higher-energy doublet. In such a situation, we can introduce the effective angular momentum for the t_{2g} levels, $l_{eff} = 1$, and the effective Hamiltonian becomes $H_{eff} = -\lambda \mathbf{l}_{eff} \cdot \mathbf{S}$. We note the opposite sign of spin–orbit coupling in comparison to the original Hamiltonian in Eq. (A.10).

We now consider the behavior of the Kramers doublets for trigonal distortions. The dependences of E_1, E_2, and E_3 on the angle θ calculated for $\lambda/\Delta_{CF} = 0.5$ and different system parameters κ and Z^* are shown in Fig. 9. Analysis shows that for considerably large λ, the energy E_3 lies above E_1 and E_2. If we neglect the effect of the neighboring magnetic ions on the crystal field ($Z^* = 0$), we obtain that $E_1 < E_2$ for the stretched ($\theta < \theta_0$) octahedra and $E_1 > E_2$ for the compressed ($\theta > \theta_0$) octahedra (see Fig. 9a,b). The contribution of the magnetic ions to the crystal field tends to make $E_1 > E_2$ (see Fig. 9c).

By considering each of three doublets separately, it is easy to demonstrate that the electron hopping integrals between the corresponding wave functions again satisfy the condition $t_{11} = t_{22} = t$, $t_{12} = 0$ and hence the exchange has the Heisenberg form, $H \sim \sim J \sum \boldsymbol{\sigma}_i \cdot \boldsymbol{\sigma}_j$, where $\boldsymbol{\sigma}$ is the effective spin describing the $j = 1/2$ doublet. However, $\boldsymbol{\sigma}$ has its own physical meaning for each doublet. This is always true for one electron or hole at the E_3 level, but in the case of E_1 or E_2, the doublets must be sufficiently far from the level-crossing point.

REFERENCES

1. J. B. Goodenough, *Magnetism and the Chemical Bond*, Wiley Intersci. New York (1963).

2. J. Chakhalian, J. W. Freeland, H.-U. Habermeier et al., Science **318**, 1114 (2007).

3. M. D. Kaplan and B. G. Vekhter, *Cooperative Phenomena in Jahn–Teller Crystals*, Plenum Press, New York (1995).

4. K. I. Kugel and D. I. Khomskii, Usp. Fiz. Nauk **136**, 621 (1982) [Sov. Phys.–Uspekhi **25**, 231 (1982)].

5. D. I. Khomskii, *Transition Metal Compounds*, Cambridge Univ. Press, Cambridge (2014).

6. S. V. Streltsov and D. I. Khomskii, Phys. Rev. B **89**, 161112 (2014).

7. K. I. Kugel, D. I. Khomskii, A. O. Sboychakov, and S. V. Streltsov, Phys. Rev. B **91**, 155125 (2015).

8. J. van den Brink and D. Khomskii, Phys. Rev. B **63**, 140416 (2001).

9. I. Affleck, Nucl. Phys. B **265**, 409 (1986).

10. Y. Yamashita, N. Shibata, and K. Ueda, Phys. Rev. B **58**, 9114 (1998).

11. B. Frischmuth, F. Mila, and M. Troyer, Phys. Rev. Lett. **82**, 835 (1999).

12. K. I. Kugel and D. I. Khomskii, Fiz. Tverd. Tela **17**, 454 (1975) [Sov. Phys.–Solid State **17**, 285 (1975)].

13. A. Abragam and B. Bleaney, *Electron Paramagnetic Resonance of Transition Ions*, Clarendon Press, Oxford (1970).

14. G. Jackeli and G. Khaliullin Phys. Rev. Lett. **102**, 017205 (2009).

15. M. V. Mostovoy and D. I. Khomskii, Phys. Rev. Lett. **89**, 227203 (2002).

16. J. Zaanen, G. A. Sawatzky, and J. W. Allen, Phys. Rev. Lett. **55**, 418 (1985).

17. G. Chen and L. Balents, Phys. Rev. B **78**, 094403 (2008).

18. S. V. Streltsov and D. I. Khomskii, Phys. Rev. B **77**, 064405 (2008).

19. Y. Singh and P. Gegenwart, Phys. Rev. B **82**, 064412 (2010).

20. K. W. Plumb, J. P. Clancy, L. J. Sandilands et al., Phys. Rev. B **90**, 041112(R) (2014).

21. A. Kitaev, Ann. Phys. (N. Y.) **321**, 2 (2006).

22. Z. Nussinov and J. van den Brink, Rev. Mod. Phys. **87**, 1 (2015).

23. K. Yamaura, H. W. Zandbergen, K. Abe, and R. J. Cava, J. Sol. St. Chem. **146**, 96 (1999).

24. S. Hirotsu, J. Phys. C **10**, 967 (1977).

25. K. E. Stitzer, M. D. Smith, J. Darriet, and H.-C. zur Loye, Chem. Comm. **17**, 1680 (2001).

26. J. Terzic, J. C. Wang, F. Ye, W. H. Song, S. J. Yuan, S. Aswartham, L. E. Delong, S. V. Streltsov, D. I. Khomskii, and G. Cao, Phys. Rev. B **91**, 235147 (2015).

27. T. Siegrist and B. L. Chamberland, J. Less-Common Metals. **170**, 93 (1991).

28. S.-T. Hong and A. W. Sleight, J. Sol. St. Chem. **122**, 251 (1997).

29. J. G. Zhao, L. X. Yang, Y. Yu, F. Y. Li, R. C. Yu, Z. Fang, L. C. Chen, and C. Q. Jin, J. Sol. St. Chem. **180**, 2816 (2007).

30. P. Köhl and D. Reinen, Z. Anorg. Allg. Chem. **433**, 81 (1977).

31. A. H. Carim, P. Dera, L. W. Finger, B. Mysen, C. T. Prewitt, and D. G. Schlom, J. Sol. St. Chem. **149**, 137 (2000).

32. C. A. Bates, P. E. Chandler, and K. W. H. Stevens, J. Phys. C **4**, 2017 (1971).

33. J. C. Slater and G. F. Koster, Phys. Rev. **94**, 1498 (1954).